Laminar Flame Speeds of Pentanol isomers: an Experimental and Modeling study

D. Natival[1], M. Pelucchi[2], A. Frassoldati[2], M. Barone[1], A. Cuoci[2], E. Ranzi[2], N. Chaumeix[1] and T. Faravelli[2]

[1] ICARE, CNRS-INSIS, Orléans, France
[2] Department of Chemistry, Materials and Chemical Engineering "G. Natta", Politecnico di Milano, Piazza Leonardo da Vinci 32, 20133 Milan, Italy

Keywords

- Laminar Flame Speed
- Alcohols combustion
- Biofuels combustion
- High temperature kinetics
- kinetic modeling

Abstract:

Long chain alcohols such as n- and iso-pentanol are foreseen as a suitable replacement for ethanol, due to more favorable physical properties (higher energy density, higher boiling point and lower hygroscopicity). The present study presents high accuracy laminar flame speed measurements for iso-pentanol/air and n-pentanol/air mixtures, at initial temperatures of 353 K, 433 K and 473 K, 1 bar pressure and equivalence ratios ranging from 0.7 to 1.5. Comparisons with previous measurements from the literature are also presented and reasons for the observed deviations are discussed in detail. The updated kinetic mechanism for alcohols combustion from the CRECK group at Politecnico di Milano is discussed and used for modeling purposes. For a more complete validation of the oxidation mechanism at high temperature conditions, modeling results are also compared with shock tube ignition delay times from the literature. This study extends the presently sparse and uncertain experimental database for high molecular weight alcohols oxidation in laminar flames, providing high accuracy and reliable experimental data of use for alcohols oxidation mechanism development and improvement.

1 Introduction

In order to decrease green-house gases and increase energetic independence, new combustion modes are currently being developed that will likely require fuel reformulation. Furthermore, regulations impose blending petroleum-based fuels with biofuels up to 20% [1]. Consequently, it is mandatory to study the impact of biofuel addition on fundamental combustion parameters and especially on pollutant emissions. Ethanol for example is widely used alone or blended with gasoline. However, ethanol is problematic due to both its source of supply and its pollutant emissions. Indeed, ethanol-gasoline and diesel blend engine-out emissions showed high concentration of carbonyl species (e.g., acetaldehyde). These compounds present an air quality concern since they are toxic and irritating, as well as being precursors to urban smog (e.g., free radicals, ozone. and peroxyacetyl nitrates) [2]. To overcome these two aspects, heavier alcohols, such as 1-pentanol and iso-pentanol, are foreseen as a suitable replacement for ethanol, constituting the next generation of biofuels. Moreover, pentanol isomers have several advantages compared to ethanol such as a higher energy density, a higher boiling point and a lower hygroscopicity [3]. Up to now, only few experimental studies were reported in the literature. Togbé et al. [4] studied 1-pentanol oxidation in a Jet Stirred Reactor (JSR) and in a 23.32 L combustion bomb. Flame speed results were presented and the unstretched laminar flame speed was derived using a non-linear relation. They also proposed a detailed chemical kinetic mechanism. Li et al. [3] measured laminar flame speeds of three pentanol isomers in a 5.35 L cylindrical vessel and used a linear relation to extrapolate the unstretched laminar flame speed. More recently, Heufer et al. [5] presented a detailed kinetic model for n-pentanol oxidation validated against ignition delay time, speciation in JSR and laminar flame speed data. For iso-pentanol, a detailed kinetic model was presented by Dayma et al. [6] and validated against speciation data from JSR. Recently, Sarathy et al. [7] developed another detailed chemical kinetic model validated against shock tube and rapid compression machine ignition delay times, speciation from JSR and counterflow premixed flame speed data.

The primary objective of the present work is to obtain new experimental laminar flame speed, with the best accuracy possible for iso-pentanol and 1-pentanol. Laminar flame speeds of iso-pentanol and 1-pentanol in air were measured, in a 56 L spherical bomb, at three initial temperatures 353, 433 and 473K. The initial pressure was fixed at 1 bar and the equivalence ratios varied from 0.7 to 1.5.

The updated mechanism for alcohols combustion from CRECK group at Politecnico di Milano (POLIMI) is discussed in Section 4 and comparisons with experimental data are reported in Section 5. The high temperature mechanism is based on previous studies on alcohol fuels[8, 9, 10, 11, 12]. A lumped kinetic mechanism has been also developed to systematically describe the low-temperature

oxidation of alcohols (1- and iso- butanol, 1- and iso-pentanol). The low temperature chemistry is beyond the scope of this study, thus it will be not discussed nor provided herein.

2 Experimental methodology

2.1 Experimental set-up

Laminar flame speeds were determined using a heated stainless steel spherical bomb made of two concentric spheres (Figure 1). The internal sphere in which the combustion is taking place has an internal diameter of 476 mm. Between the two spheres, a heat transfer fluid heats the apparatus to the desired temperature and a thermal insulation ensures a homogeneous temperature (±0.8 K). The temperature is measured via a thermocouple on the side of the inner wall of the vessel. The maximum operating pressure is 50 bar and a piezo-electric pressure transducer (Kistler 601A) equipped with a flame arrestor is used to monitor the pressure during combustion.

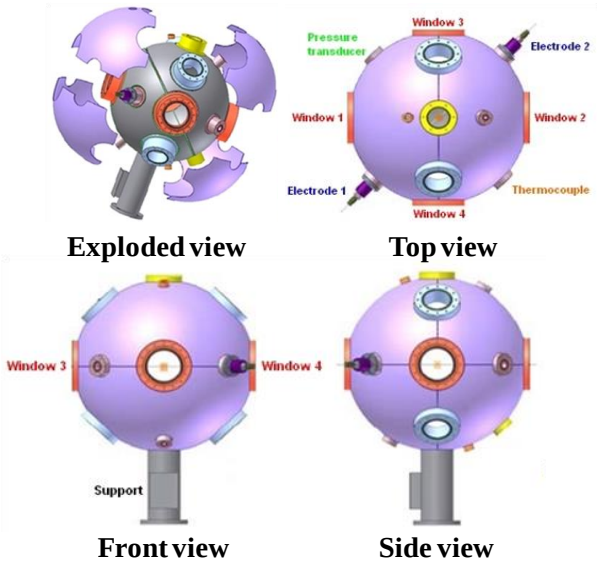

Figure 1: Exploded, top, front and side views of the spherical bomb

The mixture is spark-ignited with two tungsten electrodes connected to a high voltage generator. High voltage and current probes are connected to an oscilloscope to measure both U and I signals and therefore calculate the energy delivered by the spark ($E = \int U.I$). The average energy delivered by the high voltage generator is 1.82 mJ with a standard deviation of 0.48 mJ. The spark triggers pressure, voltage, current, and camera measurements at the same time via the oscilloscope and a TTL generator. The spherical bomb is equipped with two opposite quartz windows (97 mm optical diameter, 50 mm thick). The visualization of the flame was obtained using a Z-shape Schlieren apparatus. A white continuous lamp is used to illuminate the flame via two lenses and two concave spherical mirrors. A high speed camera (PHANTOM V1610), with an acquisition rate of 25000 images per second records

the Schlieren images of the growing flame. The frame size was fixed to a 768 × 768 pixels^2. More details can be found in [13]. A schematic of the Z-shape Schlieren configuration and the experimental setup is given in Figure 2.

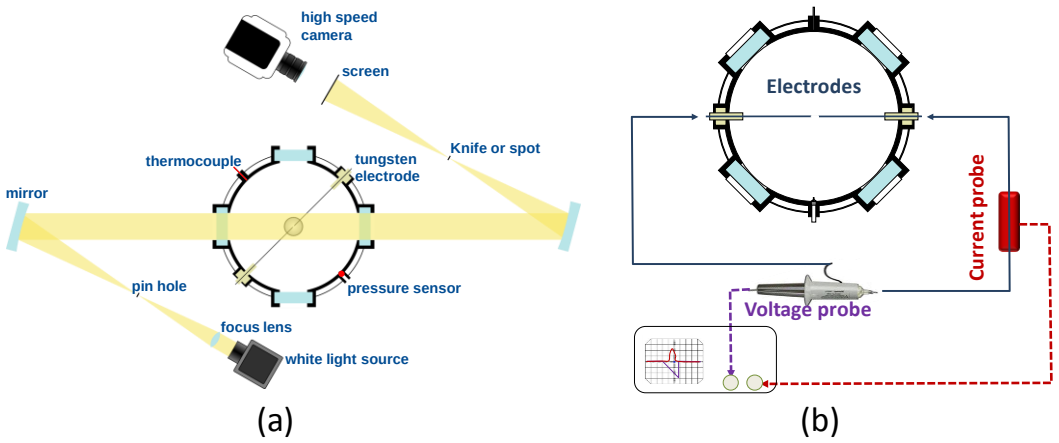

Figure 2: (a) Z-shape Schlieren configuration for the spherical flame imaging and recording; (b) Experimental setup scheme with the ignition system.

Before the introduction of the mixture, the whole setup bomb and lines were evacuated using two primary pumps. The mixtures were prepared inside the spherical bomb using 1-pentanol (Sigma Aldrich Reagentplus®≥ 99%) or iso-pentanol (Sigma Aldrich anhydrous ≥ 99%) and dry air (Air Liquide, alphagaz 2 : 20.9% O_2+ 79.1% N_2). The manufactured bottles of liquid fuel were transferred under argon atmosphere on vial equipped with septum to avoid any adsorption of water vapor in the fuel. The liquid fuel was firstly injected into the bomb with a syringe. Then, the air was introduced, creating turbulence that ensured a good mixing. Partial pressures of fuel as well as dry air were measured using capacitive manometers (MKS) of two different scales (133 and 1333 mbar). According to the precision of the manometers, the mixtures were obtained with an accuracy of 0.2%.

2.2 Laminar flame speed determination

2.2.1 Data acquisition and processing

The Schlieren images of the growing flame (Figure 3a) have been processed using a home-made code based on Matlab® [14] to obtain the radius of the flame R_f as a function of time.

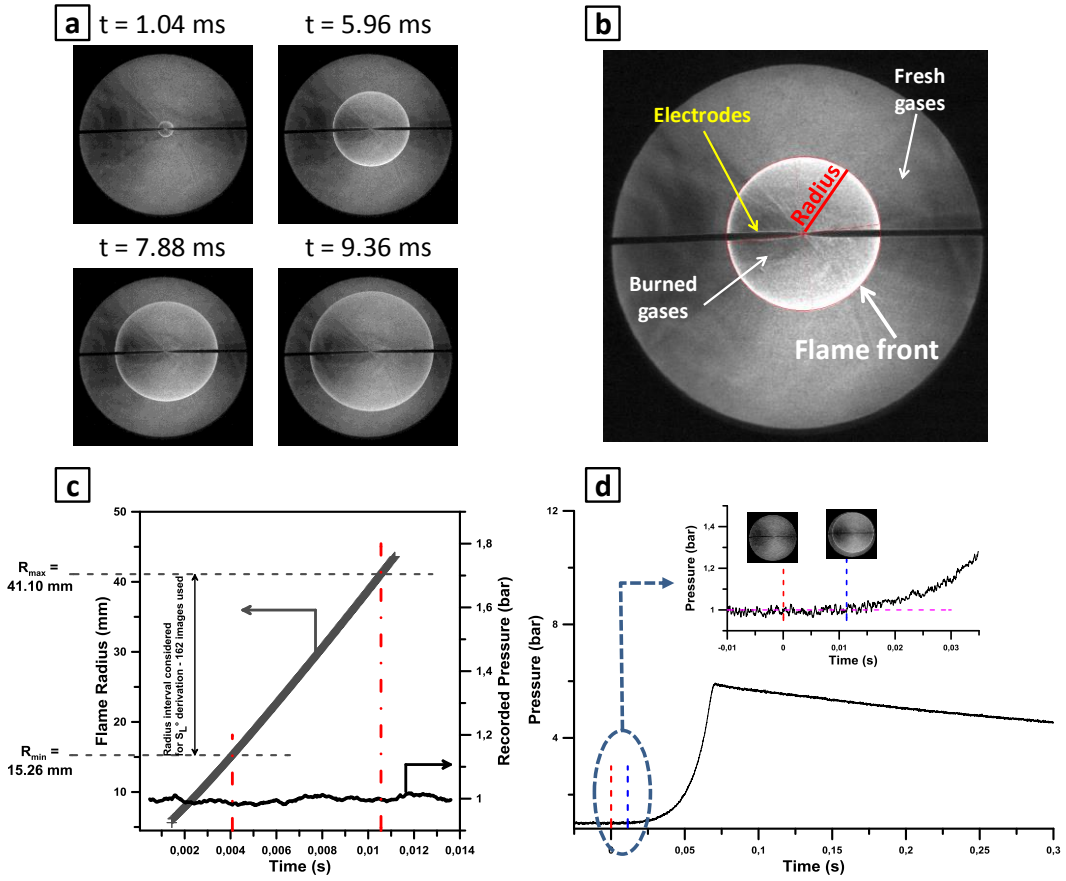

Figure 3: a) Typical propagation of the flame. b) Typical view of a Matlab process image. c) Radius of the flame as a function of time. d) Evolution of the pressure. The mixture studied here is the following: 2.84% i-$C_5H_{11}OH$/ 20.31% O_2/ 76.86% N_2 (%v/v) at initial temperature and pressure of 473K and 1 bar, respectively.

The good sphericity of a flame depends on several parameters. In the present study a special care has been taken to optimize the electrodes configuration (diameter and interdistance) to minimize the flame-electrodes interactions which can have a noticeable impact on the sphericity. This optimization aimed also to minimize the energy-deposition. Indeed, as explained by Halter et al. [15], after the spark discharge, an outward-propagating shock wave is created, followed by a slower thermal wave. The flame front possesses a high propagation speed, which rapidly decreases to reach an unaffected propagation speed.

The edge of each flame is obtained using a home-made routine based on Matlab image processing tools. The edge of the window is used to derive the scale conversion from pixel to mm. Hence, for each recorded image, an average radius is derived and the sphericity of the flame is checked (Figure 3b and 3c). After the extraction process of the flame radius versus time, the spatial flame speed $V_S = dR_f/dt$ can be determined. However, the spherical shape of the flame has to be considered since the curvature of the flame induces a stretch rate. In the case of a spherical expanding flame, the stretch rate, κ, is well defined and is given by the following expression:

$$\kappa = 2\left(V_S / R_f\right) \qquad (1)$$

Thus it is necessary to apply a stretch correction to the velocity either using a non-linear or a linear extrapolation. The early analysis of Clavin [16] and Matalon [17] led to consider that, for a relatively weak stretch rate, the laminar flame speed varies linearly with the global stretch rate according to the following expression:

$$V_S = V_S^0 - L_b \cdot \kappa \tag{2}$$

where V_S^0 is the unstretched spatial flame speed, κ the strech and L_b the Markstein length. L_b is a parameter characterizing the effect of the stretch on the flame propagation. Later, Ronney and Sivashinsky [18] showed that when the stretch is weak, a non-linear relationship exists between the stretched laminar flame speed and the stretch rate according to:

$$\left(V_S/V_S^0\right)^2 \ln\left(V_S/V_S^0\right)^2 = -2\left(L_b \cdot \kappa / V_S^0\right) \tag{3}$$

Using equation (2) leads to an overestimation of the unstretched V_S^0. In this work, the non-linear equation has been used in order to obtain the unstretched spatial flame speed and the corresponding Markstein length. Only some flame speeds of n-pentanol/air mixtures have been extrapolated with the linear relation for a fair comparison with previous data from the literature. Finally, the unstretched laminar flame speed S_L^0 is derived from the expression of Eschenbach and Agnew [19] :

$$S_L^0 = \left(V_S^0 + \frac{R_f}{3.P_b} \cdot \frac{dP_b}{dt}\right)\left(\frac{M_b}{M_u}\right)\left(\frac{T_u}{T_b}\right)\left(\frac{P_b}{P_u}\right) \tag{4}$$

where, the subscripts “u” refers to “unburned” and “b” to “burned”, M is the molar mass, T the temperature, P the pressure and t the time. By considering the initial phase of the flame propagation where the pressure does not vary yet, the term $\left(R_f/3.P_b\right)\cdot dP_b/dt$ of the relation (4) is zero. Indeed, in our experiments, at the end of the observation of the flame expansion zone, the burnt volume is about 0.8% of the total volume of the vessel and the pressure remains constant during the visualization of the propagation of the flame as shown in Figure 3d. Therefore pressure is not affecting flame propagation. Consequently the relation (4) becomes the simple equation $S_L^0 = V_S^0/\sigma$, where $\sigma = \rho_u/\rho_b$ and ρ_u, ρ_b are the unburned and burned density of the mixture, respectively. The density of unburned and burned gas ρ_u and ρ_b was calculated using COSILAB® [20] software with the Equilibrium code. All the species included in Togbé et al. [4] mechanism (for n-pentanol) and Sarathy et al. [7] mechanism (for iso-pentanol) were considered.

Despite the strong stretch at the early stage of the flame propagation due to the small radius (implying a large curvature), at the end of the propagation the stretch is supposed to asymptotically approach zero in an unconfined environment. In this study, a large spherical bomb is used allowing a flame speed extraction over a wide domain of radius (until 43 mm) and hence lower the stretch rate seen by the flame. Consequently a relatively low stretch rate can be obtained at the end of the visualization.

Moreover, the flame is analyzed for a minimum radius where the flame stretch is not anymore influenced by the spark discharge and the stretch is weaker. Finally, to exclude any influence of the ignition energy and the chamber confinement effects [21, 22], only spherical flame images with radii between 15 mm and 43 mm have been considered in this study. An example of unstretched spatial laminar burning speed extraction is given in Figure 4 with both the linear and the non-linear extraction methods. A comparison with the experimental measurement is also given.

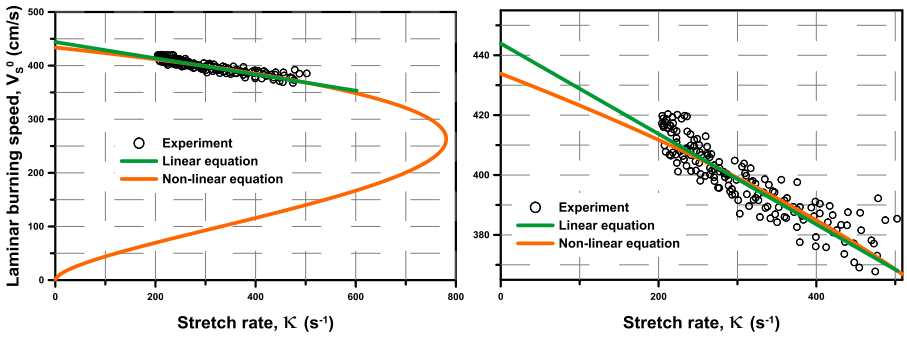

Figure 4: a) Evolution of the spatial laminar burning speed versus stretch rate b) Zoom of the evolution of the spatial laminar burning speed versus stretch rate. The mixture studied here is the following: 2.84% i-$C_5H_{11}OH$/ 20.31% O_2/ 76.86% N_2 (% v/v) at initial temperature and pressure of 473K and 1 bar, respectively.

2.2.2 Error assessment

The primary objective of this study is to rigorously measure laminar flame velocities with a minimum experimental uncertainty. As previously mentioned, to achieve results of high accuracy, the experiment were conducted: i) with pressure, temperature and composition of the mixture well known and controlled (ΔP_{ini} = ± 0.1 mbar, ΔT_{ini} = ± 0.8 K ; $\Delta\varphi$ = ± 0.2%); ii) in an extraction domain where the stretch is weak enough (R_{min} = 15 mm); iii) at perfectly constant pressure with no impact of the vessel's walls (R_{max} = 43 mm). Consequently, if these requirements are met, the main uncertainty on the determination of the laminar burning velocity comes from the estimation of the radius and on the repeatability of the experiments.

Indeed, the flame speed is directly linked to the flame radius via $V_S = dR_f/dt$. As already mentioned, each radius is determined via the Matlab® code from the images of the propagation of the flame. The dimension of the images is given in pixels. The corresponding uncertainty on the determination of the radius is ± 1 pixel. Thus, adding and subtracting one pixel on each radius on the linear or non-linear extrapolation of the flame speed, the flame speed is determined ΔU_{radii} = ± 0.90% of uncertainty.

The uncertainty linked to the global experiment was also evaluated. Indeed, in this study, to establish a curve of $S_L°$ as a function of the equivalence ratio, each experiment was repeated twice. To evaluate the repeatability, for an initial temperature of 433 K, the experiments were repeated with an

uncertainty on the temperature of ± 0.8K around 433K. The results are reported in Figure 5. An uncertainty, $\Delta U_{repeatability}$ = ± 0.4% maximum was determined with this set of experiments.

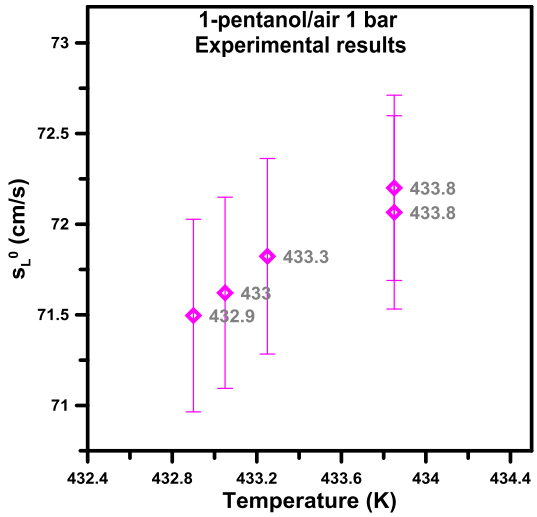

Figure 5: Evolution of the unstretched laminar burning speed versus temperature. The uncertainty lines correspond to the uncertainty of the radius determination.

Using the errors propagation formula for independent uncertainties [23]:

$$\Delta U_{global} = \sqrt{\left(\Delta U_{radii}\right)^2 + \left(\Delta U_{repeatability}\right)^2} \quad (5)$$

The global uncertainty of the flame speed for this study is 1% maximum.

3 Results and discussion

3.1 Experimental results

During this study, three initials temperatures were examined for each fuel: 353, 433 and 473 K and the initial pressure was kept constant at 1000.0 ± 0.1 mbar. Different equivalence ratios ($0.7 \leq \varphi \leq 1.5$) were tested. This domain of equivalence ratios was chosen in order to keep the domain of study identical independently from the initial temperature. The lean limit ($\varphi = 0.7$) was chosen in order to successfully obtain ignition and the rich limit ($\varphi = 1.5$) to avoid the domain where the flame wrinkling occurs. As can be observed in Figure 6a, the unstretched laminar burning velocity is maximum for all the mixtures just above stoichiometry ($1.05 \leq \varphi \leq 1.10$) and decreases with either increasing or decreasing equivalence ratios. As expected, the flame speed also increases with increasing initial temperature. Moreover, the impact of the temperature on S_L^0 depends on the equivalence ratio. Following the classical formulation [13], the exponent over the temperature can be deduced:

$$\left(S^0_{l\,(T_i)} / S^0_{l\,(T_0)}\right) = \left(T_i / T_0\right)^{\alpha} \quad (6)$$

Where the subscript "0" refers to the values at reference conditions (353 K and 1 bar in this study), "i" refers to the values at the expected conditions and α is the power exponent over the initial temperature. Figure 6b shows the α exponent derived from our measurements as function of φ. Error bar uncertainties were obtained by the least-squares procedure.

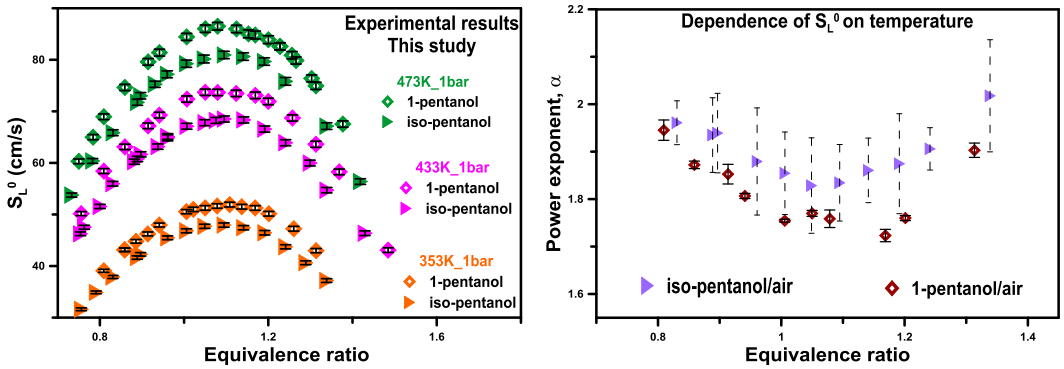

(a) (b)

Figure 6: a) Evolution of the laminar flame speed versus the equivalence ratio for 1-pentanol/air and iso-pentanol/air mixtures; b) Dependence of the exponent α on the equivalence ratio from experimental results.

Figure 7 shows the Markstein lengths L_b' versus the equivalence ratio, where $L_b' = \rho_u/\rho_b L_b$. Figures 7a and 7b compare the Markstein length at three different temperature for iso-pentanol /air and 1-pentanol/air mixtures respectively. For all considered conditions, L_b' is positive indicating that the flame is stable over the entire equivalence ratio domain. Moreover, the temperature dependence can be noticed for both mixtures. L_b' increases with increasing the temperature. Figure 7c and 7d compare L_b' for iso-pentanol and n-pentanol at the three investigated temperatures. Both fuels exhibit similar Markstein lengths over the whole investigated domain, both in terms of mixture composition and initial temperature indicating a similar response to the stretch. From an engineering perspective this means that the use of 1-pentanol in an engine would be more efficient. In fact, given the similar response to the stretch, 1-pentanol flame would be always faster to propagate.

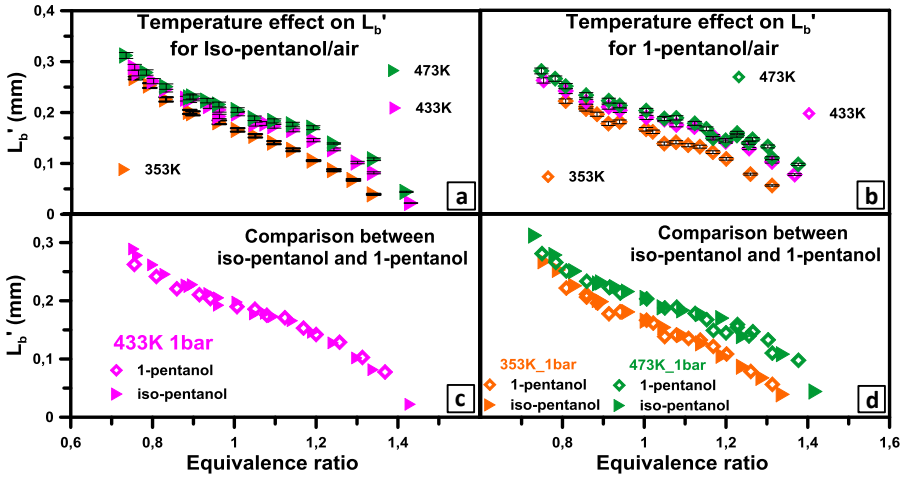

Figure 7: a) Effect of the temperature on the Markstein length for iso-pentanol/air mixtures; b) Effect of the temperature on the Markstein length for 1-pentanol/air mixtures; c) Evolution of the Markstein length versus the equivalence ratio for 1-pentanol/air and iso-pentanol/air mixtures at 433 K; d) Evolution of the Markstein length versus the equivalence ratio for 1-pentanol/air and iso-pentanol/air mixtures at 353 and 473 K.

3.2 Comparison with literature

Figure 8a compares experimental laminar flame speeds of iso-pentanol/air mixtures at 353 K from this study with the data of Sarathy et al. [7] obtained with the counterflow configuration. Despite the overall reasonable agreement, minor discrepancies are observed. In fact Sarathy et al. [7] data are shifted towards leaner regions of ~$\Delta\varphi$=0.05 compared to the present study.

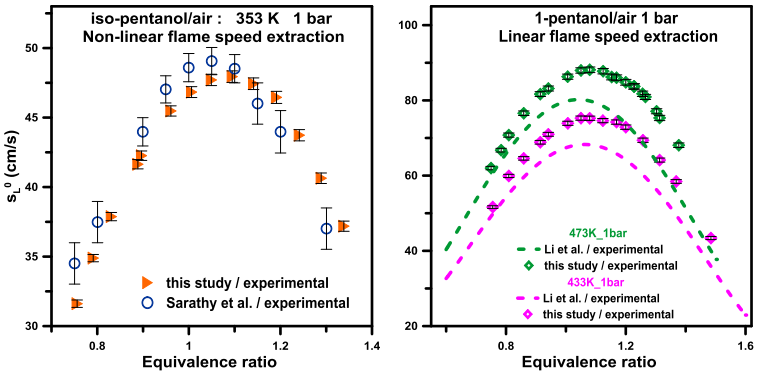

Figure 8: a) Comparison of the experimental laminar flame speed for iso-pentanol/air mixtures with Sarathy et al. [7]; b) Comparison of the experimental laminar flame speed for 1-pentanol/air mixture with Li et al. [3]. Note that the data of Figure 8b from this study (symbols) have been extracted with the linear method to be fairly compared with those of Li et al. [3].

Results for 1-pentanol/air mixtures at 433 and 473 K are compared to the data of Li et al. [3] in Figure 8b. The data are in good agreement for φ= 0.7 but a clear divergency is observed beyond this point.

The large discrepancy between the results of Li et al. [3] and the present study can be explained on the ground of many reasons. First of all, the combustion vessel used in Li et al. [3] is cylindrical with a volume of 5.35 liters and the propagation of the flame is monitored until a radius of 25 mm. Consequently, the burnt volume is about 7.85% of the total volume of the vessel and the pressure does not remain constant anymore during the visualization of the flame propagation. Secondly, the wall-effects are of importance especially in a cylindrical shape configuration, inducing a reduction in the final laminar flame speed value. Moreover, the velocity extrapolation method adopted in Li et al. [3] is linear between 6 and 25 mm flame radius. Finally, the impact of the initial conditions such as initial temperature and air composition as to be considered. No detailed discussion about these aspects is presented in Li et al. paper [3].

To understand these discrepancies many parameters were analyzed to help in highlighting their effects. First of all, the purity of the fuel was verified with an experiment performed using a new bottle of 1-pentanol, opened under a glove-box in an inert argon atmosphere. Secondly, an experiment allowing 10 minutes of waiting time before ignition was carried out to closely reproduce the experimental procedure applied by Li et al. [3]. As reported in Figure 9, no differences with our previous measurements can be observed, clearly proving that the difference between the two studies does not reside in the experimental procedure nor in the purity of the liquid fuel. Indeed, after both tests the measured flame speed at Φ=1.0 was 72.07 ± 0.72 cm/s.

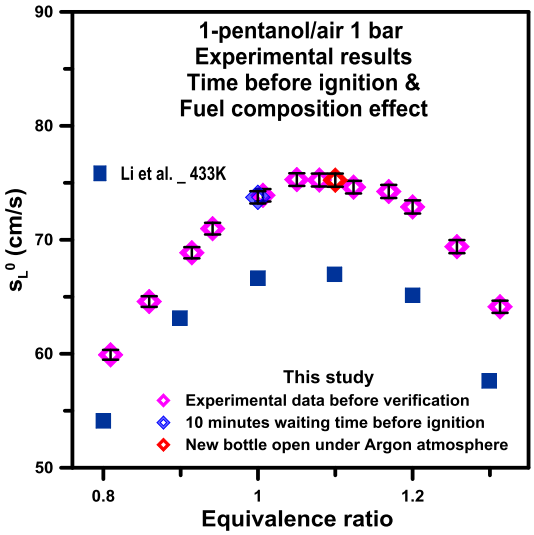

Figure 9: Effect of fuel composition and waiting time before ignition on S_L^0. Experiments performed at 433K, 1bar.

Laminar flame speed of 1-pentanol/air mixtures were also measured by Togbé et al. [4] at 423 K and 1 atm. The non-linear method was used to extract the speed value. Therefore, a few experiments were performed at 423 K in this study, in order to fairly compare the results of Togbé et al. with our data. As shown in Table 1, a large discrepancy between the two measurements is observed. After discussion with the authors of Togbe et al. paper, it was concluded that one of the reason of the observed

deviations resides in the different composition of air. In fact a 20.5% O_2-79.5% N_2 in volume synthetic air was used in Togbé et al. [4].

To identify the effect of air composition on the flame speed, additional experiments have been performed. Different observations can be extrapolated from the results reported in Table 1. With regards to the comparison with Li et al. [3] measurement at 393 K, 1 bar and φ=1.0: i) their measurement lies in between the 20.9% and the 20% O_2 cases analyzed in this study, in both cases the deviation is in the order of ±4 cm/s ii) the two measurements carried out over different flame radius (15-43 mm and 6-25 mm) with the same air composition agree within ± 1 cm/s with one another. It can be concluded that the discrepancies between the results from different studies most probably depend on the pressure variation in a small combustion chamber. Concerning the comparison at 423 K, 1 atm and φ~1.1 the use of a 20% O_2 synthetic air lead to a better agreement with the measurement of Togbè et al. [4] but still the flame speed value from the present study is ~3 cm/s higher.

	Air composition	**Temperature & pressure**	**Flame radius range**	**Extrapolation Method**	**S_L^0 (cm/s)**	**Φ**
This study	20%O_2 / 80%N_2	393K / 1 bar	15-43mm	Linear	54.78 ± 0.36	1.00
This study	20.9%O_2 / 79.1%N_2	393K / 1 bar	15-43mm	Linear	62.18 ± 0.42	1.00
This study	20.9%O_2 / 79.1%N_2	393K / 1 bar	6-25 mm	Linear	63.27 ± 0.35	1.00
Li et al. [3]	Not reported	393K / 1 bar	6-25 mm	Linear	58.75	1.00
This study	20%O_2 / 80%N_2	424.0 K / 1 atm	15-43mm	Non-linear	63.82±0.48	1.10
This study	20.9%O_2 / 79.1%N_2	424.5 K / 1 atm	15-43mm	Non-linear	70.30± 0.54	1.10
Tobgé et al. [4]	20.5%O_2 / 79.5%N_2	423 K / 1 atm	Not reported	Non-linear	60.95	1.11

Table 1: Effect of the air composition and post process radius range on S_L^0. Comparison with Togbé et al. and Li et al. at respectively 423 K, 1atm and 393 K, 1 bar for 1-pentanol/air mixtures.

4 High temperature Kinetic Mechanism

Figure 10 and 11 show simplified primary decomposition mechanisms of *1*-pentanol and *iso*-pentanol respectively. Radical chain initiates at high temperature via unimolecular initiation reactions leading to the formation of two radical species. Both C-C and C-H bond breakings (not reported in Figure 10 and 11) are included in the mechanism here discussed. Molecular dehydration and dehydrogenation reactions involving a four center cyclic transition state lead to the formation of corresponding alkene or aldehyde respectively. Six different radicals are generated via H-abstraction reactions from *n*-pentanol. Only five radicals are considered for *iso*-pentanol due to symmetry of the primary δ positions (6 primary hydrogen available for H-abstraction). These radicals can isomerize via 5-, 6- or 7-member ring intermediates or decompose via β-decomposition reactions to smaller radicals and unsaturated species. Beside the fuel specific reactions, consumption pathways for important intermediates have been included. For the unsaturated alcohols (n- and i-pentenol) kinetic parameters are based on smaller enols already included in the mechanism. It has to be noticed that a single species representative of all the possible isomers is considered for n- and iso-pentenol. Aldehydes specific reactions are from a recent study of the high temperature oxidation of *n*-C_3-C_5 aldehydes [24]. While high temperature kinetics for n-pentanal were already included in the mechanism, rate parameters for iso-pentanal were derived based on analogy rules.

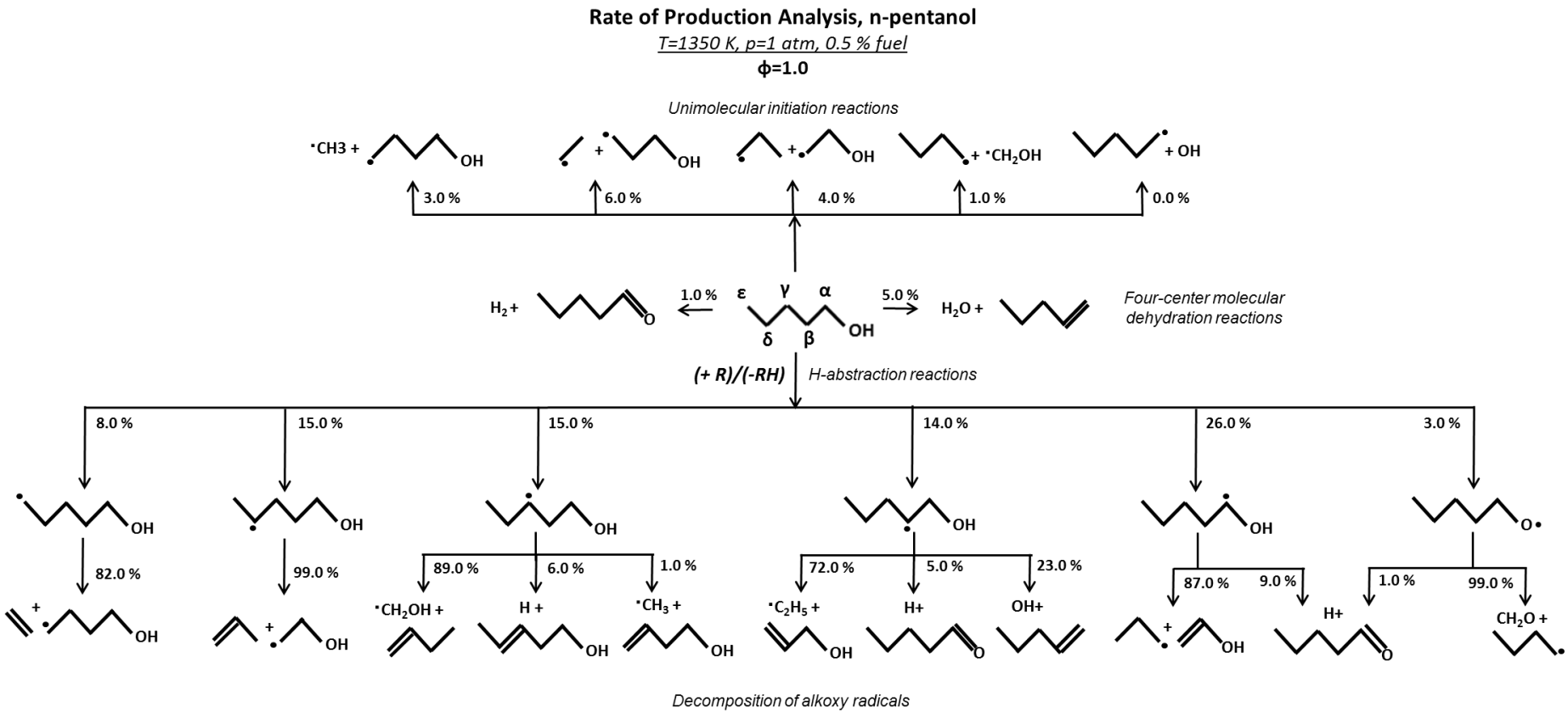

Figure 10: Primary decomposition reactions of n-pentanol. Unimolecular initiation reactions involving C-H bond breakings and isomerization channels have been omitted for claritity. Global reaction path analysis for n-pentanol at 1350 K, 1 atm, φ=1.0. Isomerization contributions can be deduced by closing the balance of individual radical decomposition channels to 100%.

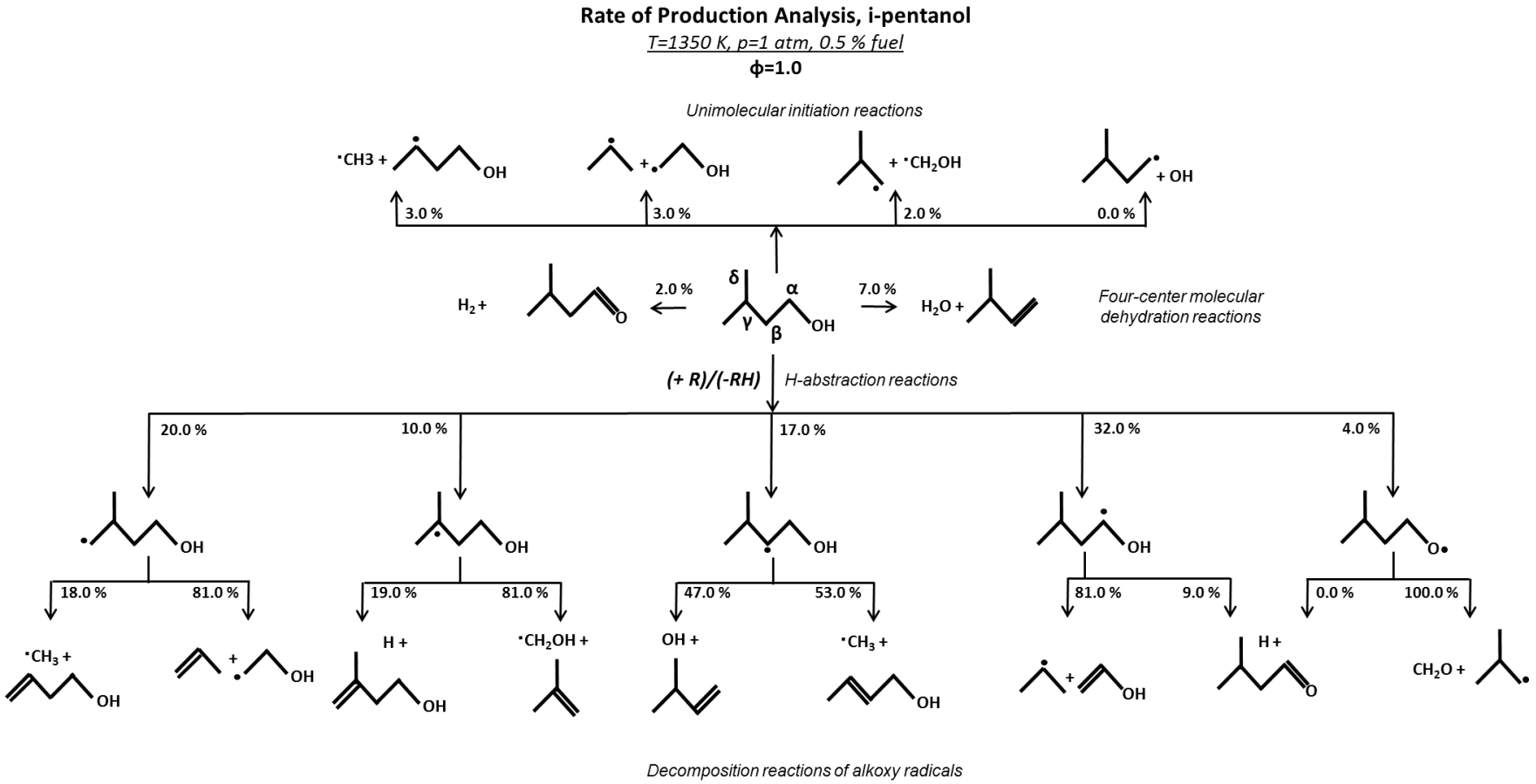

Figure 11: Primary decomposition reactions of iso-pentanol. Unimolecular initiation reactions involving C-H bond breakings and isomerization channels have been omitted for claritity. Global reaction path analysis for iso-pentanol at 1350 K, 1 atm, φ=1.0. Isomerization contributions can be deduced by closing the balance of individual radical decomposition channels to 100%.

Unimolecular intitiation reactions

CBS-QB3 calculations were carried out by Zhao et al. [25] to systematically investigate the dominant reaction channels of the thermal decomposition of three pentanol isomers: *n*-pentanol (1-pentanol), 2-methyl-1-butanol, 3 methyl-1-butanol (*iso*-pentanol in this study). Subsequently the same authors computed temperature and pressure dependent rate constants by RRKM/ME. Figure 12 shows a comparison of the high pressure limit rate constants as calculated by Zhao et al. [25] and those included in the kinetic mechanism of POLIMI here discussed. Activation energies are consistent with the previous study on butanol isomers by Grana et al. [10], frequency factors have been updated to improve agreement with values from Zhao et al. An average factor of ~2 is observed between proposed rate constant values and those adopted in this study. Relative selectivities to the different channels involving a C-C bond breaking at 1500 K are also reported in the graph, showing good agreement between the two sets of rate constants.

Similar deviations, still within kinetic uncertainty, are also observed for *iso*-pentanol decomposition reactions. A recent study by Sarathy et al. [7] highlighted the need to increase the A factor (10 times) for the reaction leading to the formation of a methyl radical and γ-hydroxybutyl radical to improve agreement with the experimental data. Considering this large uncertainty, the rate constant proposed by Grana et al. [10] for the analogous channel of *iso*-butanol has been increased of a more careful factor 3.5, as detailed in Figure 13. Moreover, also shown in Figure 13, a correct activation energy of ~88 kcal/mol was proposed by Grana et al. prior to any detailed calculation was available in literature. The total decomposition rate constant is also reported bottom right of Figure 12.

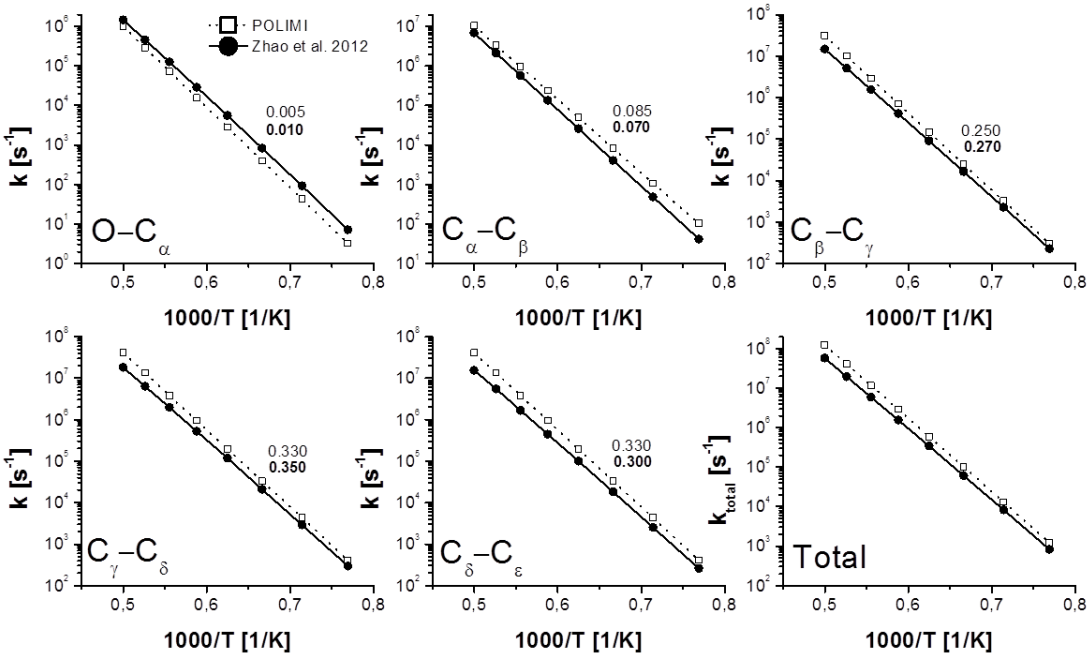

Figure 12: High pressure limit rate constants (s^{-1}) for n-pentanol decomposition channels, and total decomposition rate constant. Comparison between values from Zhao et al. [25] and those adopted in this study. Values reported inside graphs represent relative selectivities of the different C-C unimolecular channels at 1500 K: this study (plain), Zhao et al. (bold).

Concerning C-H bonds the presence of the hydroxyl moiety weakens the adjacent C_α-H (~95 kcal/mol) with respect to a secondary C-H in alkanes (~99 kcal/mol). As a consequence C_β-H bonds are slightly stronger than the corresponding bond in alkanes of (~1-2 kcal/mol) [26], while C_γ-H are not strongly influenced by the presence of the OH group. The O-H Bond Dissociation Energies (BDE) are high for every alcohol fuel (~105 kcal/mol), therefore unimolecular reactions involving the scission of this bond do not significantly contribute to fuel decomposition. Despite unimolecular reactions involving the breaking of a C-H bond are less important, they are all included in the mechanism because of the possible influence on flame propagation. The same reference kinetic parameter for the reverse recombination reaction

H+R' = R'H $\qquad k = 5.0 \times 10^{13}$ [cm^3 mol^{-1} s^{-1}]

is adopted, where R'H is the fuel molecule, R' the fuel radical derived from the C-H fission.

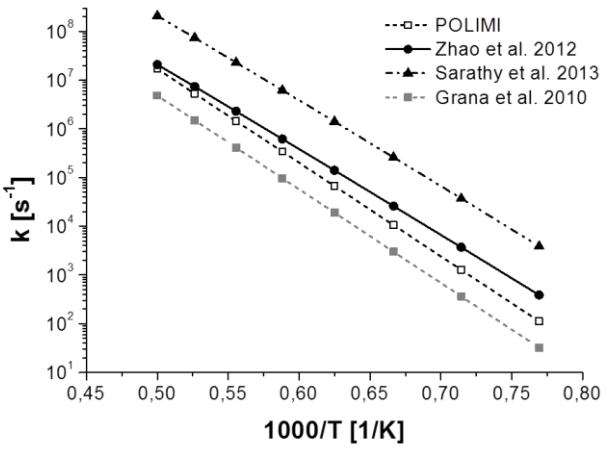

Figure 13: Rate constant [s^{-1}] of the decomposition of iso-pentanol to methyl radical and γ-hydroxybutyl radical. Comparison between values from Zhao et al. [25], Sarathy et al. [7], Grana et al. [10] (iso-butanol) and that adopted in this study.

H-abstraction reactions

Rate parameters of H-abstraction reactions are based on the systematic approach described elsewhere [27]. As reported in Grana et al. [10], the kinetic parameters for the H-abstraction from the hydroxyl group are assumed to be equal to those of a primary H atom from a methyl group. To account for the weakened C_α-H bond discussed in the previous section, the reference kinetics for a secondary site in alkanes have been increased of 50%. Remaining primary, secondary and tertiary sites are treated according to alkanes rules in their general form of R+R'H=RH+R', where R'H is the fuel molecule and R is the generic abstracting radical.

H-abstractions by H, OH and HO_2 have been carefully considered, being dominant paths over the conditions explored in this study. Figure 14 shows relative selectivities of metathesis reactions by H, OH and HO_2 as adopted in this study (panel a and b) and those from similar study on *n*- and *iso*-pentanol (panel c and d) [5,7]. Consistently with C-H BDEs discussed in the previous section, abstraction from the α-site dominates for both fuels, β-sites are slightly less selective than an alkane-like secondary H-atom abstraction (i.e. γ-site and δ-site for *n*-pentanol) and more selective than the single tertiary H-atom available at the γ-site for *iso*-pentanol. Lower contributions to the fuel decomposition through H-abstraction are those coming from the O-H group. Selectivities on primary ε (*n*-pentanol) and δ (*iso*-pentanol) are respectively ~3 times and ~6 times higher than that of the primary H-atom of the hydroxyl moiety.

According to Heufer et al. [5] 70% of the abstracting HO_2 reacts at the α-site for *n*-pentanol resulting in a much lower selectivity on secondary β and γ sites. In general, a more homogeneous distribution between secondary sites is observed in *n*-pentanol selectivities from this study compared to those of Heufer [5]. Good agreement between the two studies is found for δ and ε positions.

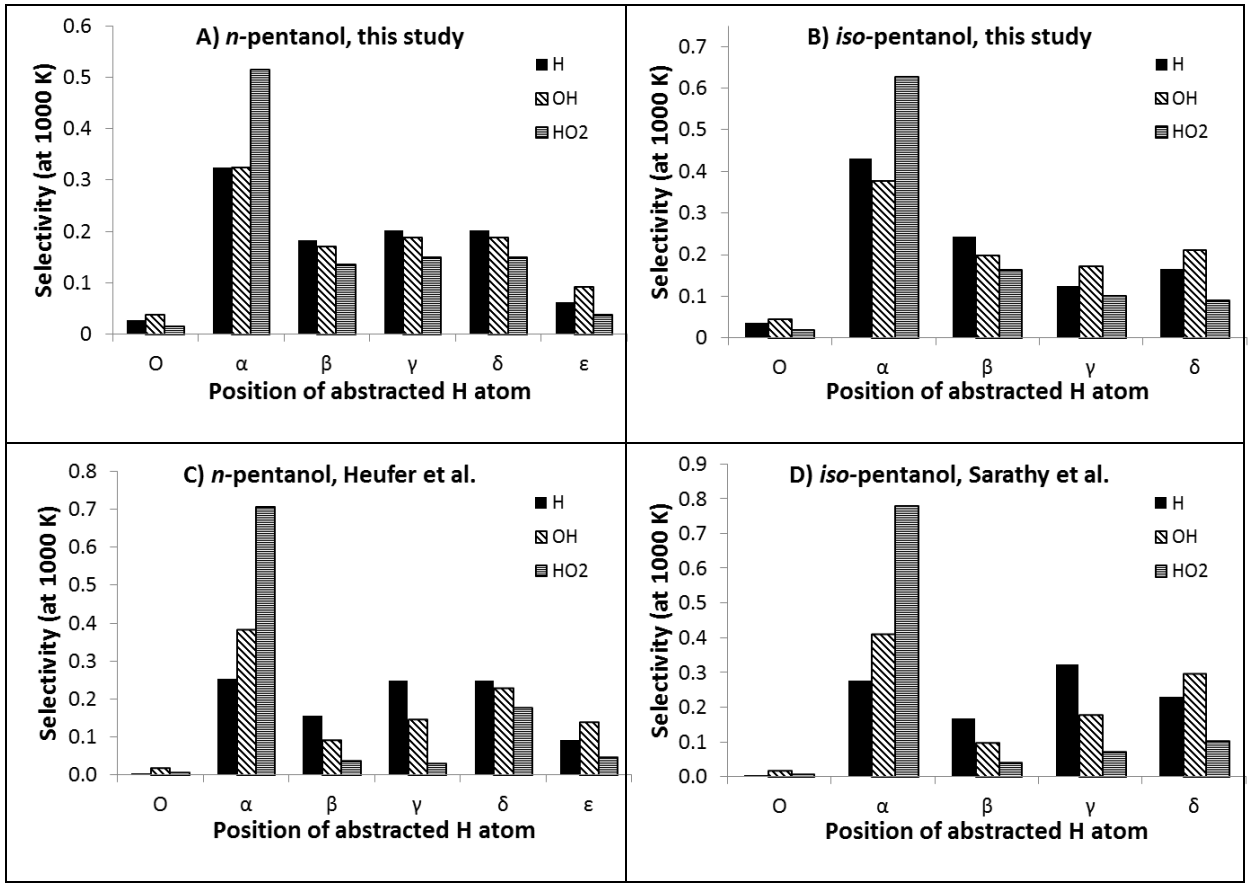

Figure 14: Selectivity of the abstracted H-atom to form primary $C_5H_{11}O$ radicals from H-abstraction reactions by H,OH and HO_2 at T=1000 K. n-pentanol (panel a) and iso-pentanol (panel b) from this study, and previous works from Heufer et al. [5] and from Sarathy et al. [7].

Similar trends are observed for the analogous α-abstraction reaction in *iso*-pentanol. According to Sarathy et al. [7], up to 80% of abstraction by HO_2 occurs at the weakened α secondary site resulting in a decreased selectivity to β. Selectivity of H-abstraction by H on tertiary γ is about twice that proposed in this study. Good agreement is found for the 6 primary hydrogen available at the primary δ position.

Table S1 in the Supplemental Material reports rate constants for hydrogen abstractions for *n*- and *iso*-C_4 and C_5 alcohol fuels, highlighting the internal consistency existing between alcohol fuels in the POLIMI mechanism.

Decomposition reactions of alkoxy radicals

Kinetic parameters of alkoxy radicals decomposition have been previously discussed by Frassoldati et al. [9]. Alkoxy radicals from primary alcohols with n carbon atoms can decompose to form a C_{n-1} alkyl radical and formaldehyde or dehydrogenate to give the corresponding C_n aldehyde. The first channel prevails over the dehydrogenation channel in the whole temperature range of interest to this study. Dehydrogenation of α-alkyl radicals leads to the formation of the corresponding aldehyde, while its decomposition produce vinyl alcohol, assumed to be instantaneously transformed into acetaldehyde via keto-enol tautomerism, and an alkyl radical. Based on analogy, reference kinetic parameters already adopted in previous studies for smaller alcohols have been adopted [9, 10]. Kinetic data for other alkyl-hydroxy radicals decomposition and isomerization are the same as those for alkanes [28, 29, 30]. Kinetic parameters for this class of reaction are reported in the Supplemental Material (Table S1).

Isomerization reactions

1-4, 1-5 and 1-6 H-transfer reactions, via 5-, 6- or 7- membered rings play a significant role at low-intermediate temperatures (700-1100 K). The number of atoms in the transition state ring structure and the type of sites involved allows estimation of rate parameters according to rules proposed by Dente et al. [30]. To account for the differences between BDEs of a standard C-H primary bond and that of an O-H bond, an extra 1.5 kcal/mol energy is accounted for when an oxygen atom is incorporated in the cyclic intermediate. The same rule was applied the previous work on butanol isomers from Grana et al. [10]. Table S1 in the Supplemental Material reports rate constants for isomerization reactions. The largest contribution to n-pentanol isomerization channels comes from the primary ε radical, turning into α secondary radical through a 6-membered ring transition state, followed by the 5-membered isomerization leading from α to δ. δ-radical also undergoes isomerization to form the alkoxy radical, via a 6-membered ring. The net result at ~1000 K is that about 70% of the ε-radical turns into the alkoxy radical and partially into the α radical. Concerning iso-pentanol oxidation, at ~1000 K about 20% of the α-radical is consumed through the internal H-abstraction reaction (5-membered cyclic intermediate) from the 6 primary hydrogen atoms sited in δ positions, this constitutes the most important isomerization channel. A non-negligible contribution also comes from the 6-membered ring isomerization turning delta into the alkoxy radical.

Four-center molecular dehydration and dehydrogenation reactions

Dehydration reactions (Figure 15) are the main source of pentene isomers in *n*- and *iso*-pentanol combustion at temperatures higher than ~1200 K. Only those proceeding via a four-center transition state ring are generally considered in alcohol kinetic models being both thermodynamically and kinetically favored according to calculations by Moc et al. [31]. Reference kinetic parameters were defined by Grana et al. [10] for reactions involving a primary OH group and a single primary H atom

$k = 5.0 \times 10^{13} \exp[-68600/(RT)]\ [s^{-1}]$

Corrections need to be applied to the reference rate constant to account for the secondary H-atom involved (-1000 cal/mol to the activation energy, factor of 2 increase to the frequency factor).

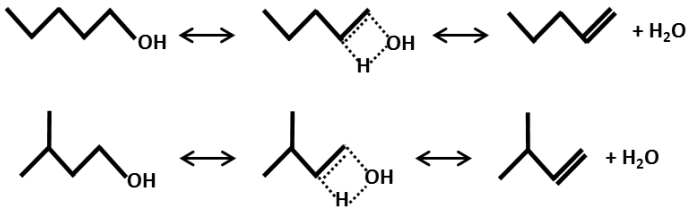

Figure 15:Dehydration reactions of n- and iso- pentanol to form 1-pentene and 3-methyl-1butene respectively.

The mechanism also includes a similar class of four-center dehydrogenation reactions leading to the formation of hydrogen and a carbonyl compound in alcohol combustion (Figure 16). In the case here analyzed dehydrogenation reactions constitute a major path to the formation of iso-pentanal and n-pentanal respectively for n- and iso-pentanol. The interest of this reaction class at high temperatures (> 1300 K) and low pressure was already discussed in the C_4 alcohols mechanism by Grana et al. [10]. Despite its important contribution to the formation of acyl compounds (aldehydes from primary alcohols and ketones from secondary alcohols) this reaction was neglected in the previous comprehensive studies on pentanol isomers by Heufer [5] and Sarathy [7]. Due to the analogous transition state configuration (see Figure 16) the same kinetic parameters are assumed for both *n*- and *iso*-pentanol.

$k = 5.0 \times 10^{13} \exp[-69500/(RT)]\ [s^{-1}]$

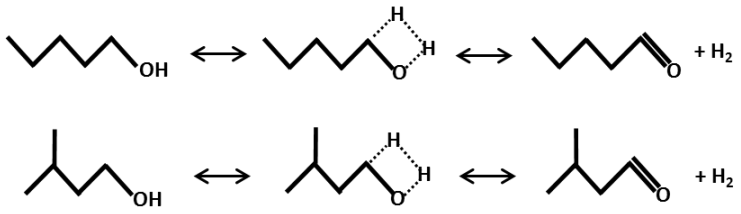

Figure 16: Dehydrogenation reactions of n- and iso- pentanol to form n- and iso-pentanal.

5 Results and Discussion

Kinetic scheme and numerical method

The oxidation mechanism used to describe the high temperature oxidation of pentanol isomers, consisting of 230 species and 7885 reactions, is available with thermo and transport properties in the Supplemental Material attached to this study and online (http://creckmodeling.chem.polimi.it). Thermochemical and transport parameters of the two isomers and related radicals were adopted from Heufer et al. [5] (n-pentanol) and from Sarathy et al. [7] (i-pentanol). All simulations were performed with the OpenSMOKE++ code by Cuoci et al. [32]. High temperature shock tube are assumed as a constant volume batch reactor. Laminar flame speeds were calculated for the steady, freely propagating, adiabatic flames in the doubly infinite domain, allowing for Soret diffusion effects. Details of the numerical method are given elsewhere [33, 34]. The normalized flame speed sensitivity coefficient s_{s_L} is used instead of the raw coefficient S_{s_L} [34, 35]

$$s_{s_L} = \frac{\delta \ln s_L}{\delta \ln \alpha} = \frac{\alpha}{s_L}\frac{\delta s_L}{\delta \alpha} = \frac{\alpha}{y} S_{s_L}$$

where s_L is the calculated mass flow rate and α the generic frequency factor.

Laminar Flame Speeds

Figure 17 shows a satisfactory comparison between the experimental data from this study and calculated atmospheric laminar flames for n-pentanol/air mixtures at three different initial temperatures. Not surprisingly, sensitivity coefficients reported in Figure 18 do not highlight any fuel specific reaction to be of importance, limiting the kinetics governing laminar flames propagation to the hydrogen-syngas-methane sub-mechanism.

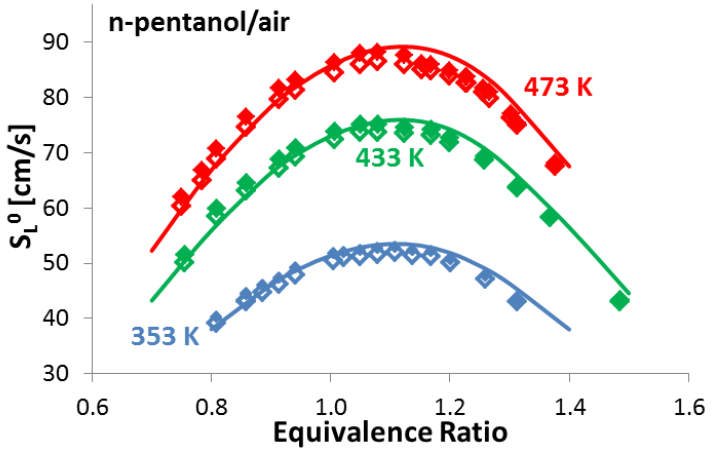

Figure 17: Laminar flame speeds of n-pentanol/air mixtures, at p=1 bar, and T_u=353 K, 433 K, 473 K. Experimental data from this study. Open symbols: non-linear stretch correction, full symbols: linear stretch correction, lines: simulations.

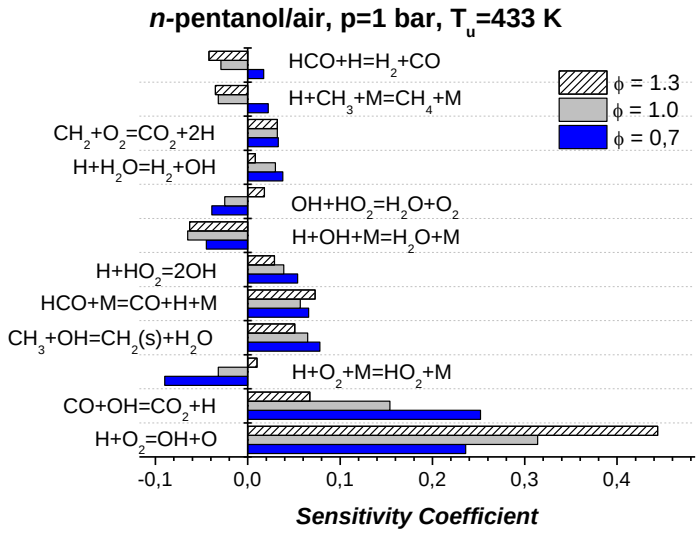

Figure 18: Sensitivity coefficients of laminar flame speed to reaction rate coefficients, for rich (φ=1.3), stoichiometric (φ=1.0) and lean (φ=0.7) n-pentanol/air flames at p=1 bar and T_u=433 K.

In Figure 19, the calculated laminar flame speeds have been also compared with previous experimental measurements from Togbè et al. [4] and Li et al. [3]. Following the discussion of Section 3.2 about Togbè et al. [4] data at 423 K, the model is able to capture the strong impact of a slightly different air composition (20.5% O_2, 79.5% N_2) on laminar flame speeds. While good agreement is found for lean to stoichiometric conditions, the model starts to deviate for φ>1.0, predicting a flame speed up to ˜11 cm/s higher than the measured value at φ=1.4. A similar behavior is observed in the case of Li et al. [3] at 433 K.

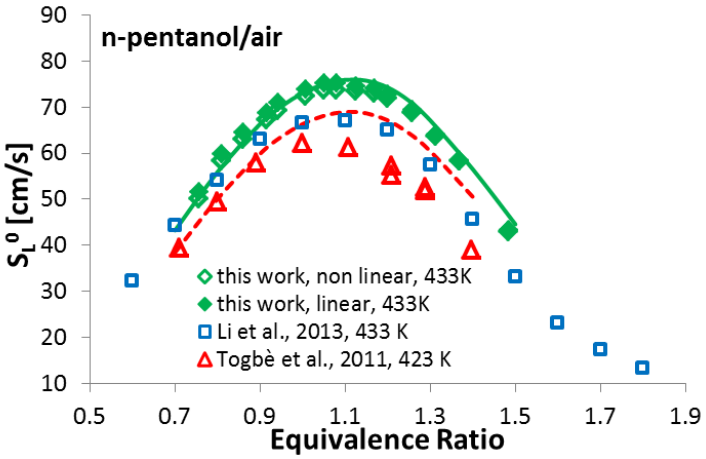

Figure 19: Laminar flame speeds of n-pentanol/air mixtures, p=1 atm, T_u=433 K. Experimental data from this study (diamonds) and from previous studies [3, 4]. Open diamonds: non-linear stretch correction (this work), full diamonds: linear stretch correction (this work), open squares: Li et al. [3], open triangles: Togbè et al. [4] (T_u=423 K). Solid line: simulation at T_u=433 K, dashed line: simulation at T_u=423 K. Simulations of Togbè et al. [4] have been performed in 20.5%O_2-79.5%N_2 air.

Figure 20 shows a comparison between measurements of Li et al. [3] at 433 K and varying pressure [0.1-0.75 MPa]. Despite the observed deviations whose possible reasons have been discussed in Section 3.2, the model is able to accurately reproduce the pressure effect on laminar flame speeds. Once again good agreement is found for lean to stoichiometric conditions.

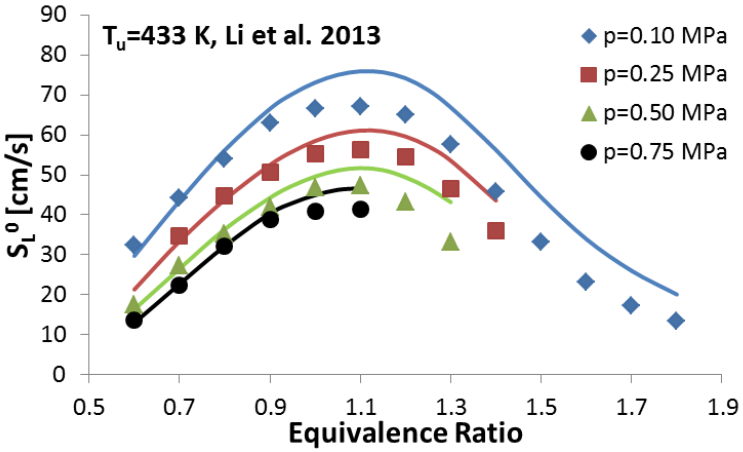

Figure 20: Laminar flame speeds of n-pentanol/air mixtures at T_u=433 K and different pressures. Symbols: experimental data by Li et al. [3], lines: simulations.

Calculated laminar flame speeds for iso-pentanol/air mixtures are compared to the experimental data from this work at three different initial temperatures and 1 bar pressure in Figure 21 showing satisfactory agreement. Data from Sarathy et al. [7] obtained in a counterflow configuration at 353 K are also reported in Figure 21. As previously observed (Section 3.2), despite an overall reasonable agreement between the two different measurements at 353 K, data from Sarathy appears to be shifted towards leaner regions, resulting in a ˜8 cm/s difference between model predictions and experimental measurements at φ=1.5.

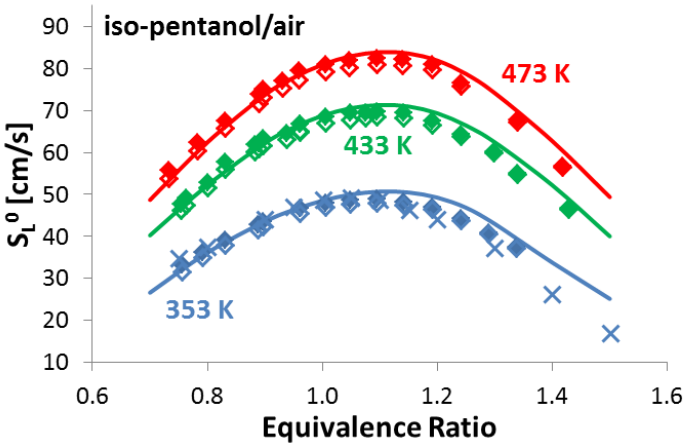

Figure 21: Laminar flame speeds of iso-pentanol/air mixtures, at p=1 atm, and T_u=353 K, 433 K, 473 K. Experimental data from this study (diamonds) and from Sarathy et al. [7] (crosses). Open symbols: non-linear stretch correction, full symbols: linear stretch correction, lines: simulations.

The same reactions previously highlighted as sensitive for n-pentanol flames are found to govern i-pentanol flame propagation, as reported in the sensitivity coefficients of Figure 22. Nevertheless,

comparing n- and iso-pentanol flame speeds at the same initial temperature conditions (433 K) in Figure 23, it can be noticed that iso-pentanol is clearly less reactive. In fact, iso-pentanol flame speeds are 3.9-5.5 cm/s slower than those of n-pentanol over the equivalence ratio range analyzed. This trend is satisfactorily reproduced by the numerical simulations as reported.

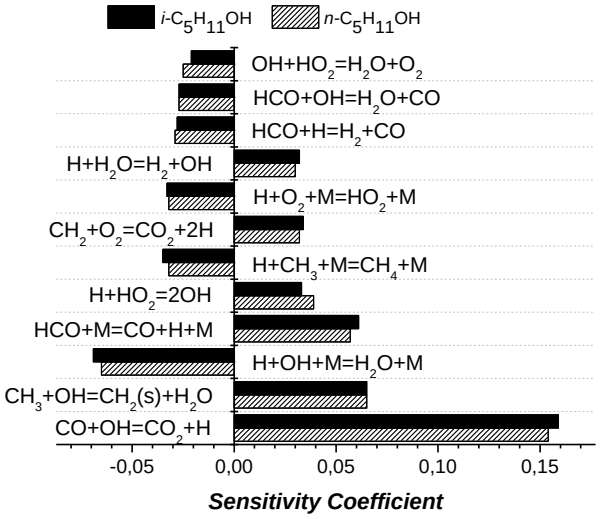

Figure 22: Sensitivity coefficients of laminar flame speed to reaction rate coefficients, for φ=1.0 n- and iso-pentanol/air flame at p=1 atm and T_u=433 K. The most sensitive reaction H+O_2=OH+O has been omitted for clarity.

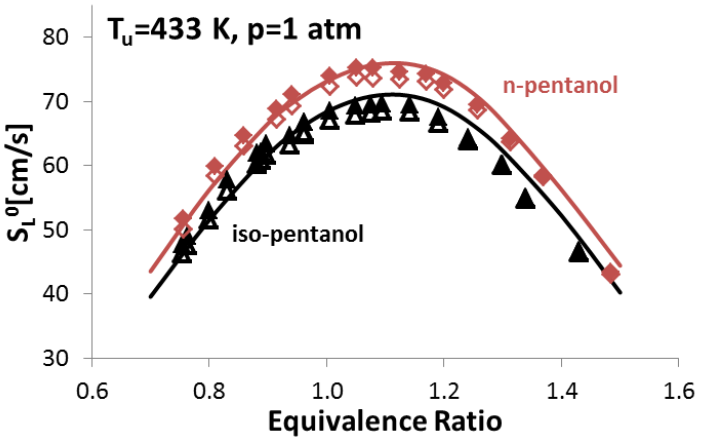

Figure 23:Laminar flame speeds of n- and iso-pentanol/air mixtures, at p=1 atm, and T_u=433 K. Experimental data from this study. Diamonds: n-pentanol, triangles: iso-pentanol. Open symbols: non-linear stretch correction, full symbols: linear stretch correction.

Since the adiabatic flame temperatures of φ=1.1 n- and iso-pentanol/air flames are very similar (~2336 K and ~2330 K at 433 K initial temperature), reasons for the different reactivity have to be found in the kinetics of the two systems. Important intermediate species profile versus the axial position in a

φ=1.1 atmospheric flame are reported in Figure 24 for both fuels. While n-pentanol mainly proceeds towards the formation of ethylene (see Figure 10), large amounts of propylene are formed in the iso-pentanol flame through the primary reactions shown in Figure 11.

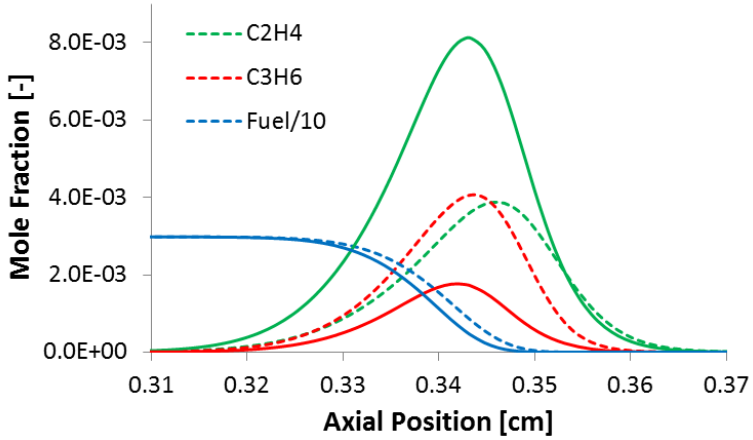

Figure 24: Species profile in a φ=1.1 atmospheric fuel/air flame at 433 K. Dashed lines: iso-pentanol, Solid lines: n-pentanol.

Similarly to what discussed by Ranzi et al. [34] comparing pure ethylene and propylene/air flames, H-abstractions by H and OH on propylene mainly produce resonantly stabilized allyl radical (aC_3H_5), resulting in a reduced flame speed. Ethylene instead is mainly converted to vinyl radical (C_2H_3) via H-abstraction. The subsequent interaction of vinyl radical with molecular oxygen ($O_2+C_2H_3=O+CH_2CHO$) is known to largely promote flame propagation. Figure 25 reports a comparison of vinyl and allyl radical profiles in n- and iso-pentanol flames.

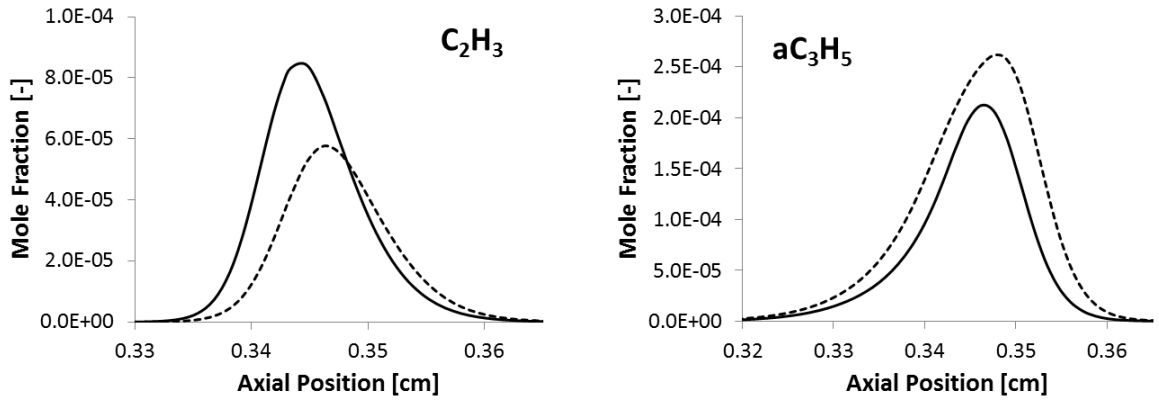

Figure 25:Radical species profile in a φ=1.1 atmospheric fuel/air flame at 433 K. Dashed lines: iso-pentanol, Solid lines: n-pentanol.

To further validate n- and iso-pentanol high temperature chemistry, model predictions have been compared with the high temperature shock tube data presented by Tang et al. [36]. Result for 0.5% fuel/O_2/Ar mixtures at 1 atm reflected pressure are shown in Figure 26. The lower reactivity of iso-pentanol is once again confirmed by both experimental measurements and model predictions. Particularly the different reactivity of the two isomers is evident at stoichiometric conditions, while for leaner conditions (φ=0.5 and φ=0.25) the ignition delay times become closer. The model is able to reasonably reproduce both the measured ignition delay times at any dilution conditions, and the relative reactivity of n- and iso-pentanol.

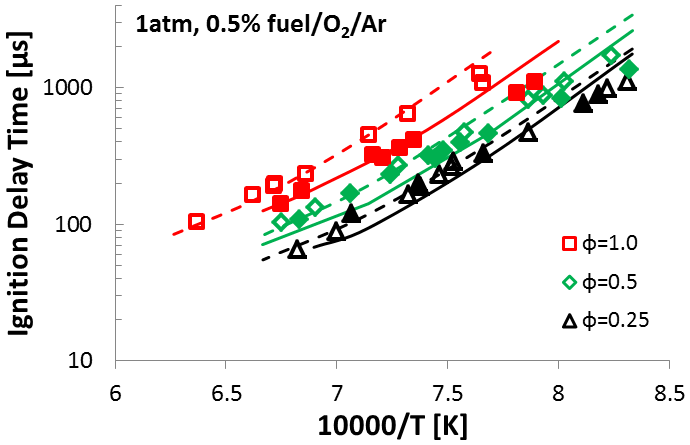

Figure 26: Ignition delay times for n-pentanol and iso-pentanol at 1 atm. Experimental data by Tang et al. [36]. Open symbols/dashed lines: i-pentanol, full symbols/solid lines: n-pentanol.

Figure 10 and Figure 11 of Section 4 also present rate of production analyses at 1350 K and 1 atm pressure, for n- and iso-pentanol/O_2/Ar stoichiometric mixtures.

Unimolecular decomposition reactions are responsible for ˜15 % of n-pentanol consumption (Figure 10), mainly occurring through the cleavage of C_γ-C_δ bond to form ethyl radical and γ-hydroxypropyl radical (·$CH_2CH_2CH_2OH$). A non-negligible contribution is given by the dehydration reaction to form 1-pentene. The most of the fuel undergoes H-abstraction, mainly by H and OH. The dominant channel is α site, followed by the secondary positions β, γ and δ. β-decomposition reactions of fuel radicals lead to the formation of smaller radicals and unsaturated species (olefins, aldehydes and enols). Isomerization contributions, of small entity under the flux analysis conditions, have not been reported

for clarity. However their relative importance can be deduced by closing the balance of fuel radical decompositions up to 100%.

Referring to Figure 11, unimolecular pathways in iso-pentanol oxidation are even of lower significance, compared to n-pentanol. A slightly larger contribution is observed for the dehydration channel, leading to the formation of iso-pentene. H-abstraction is largely dominated by the alpha channel, closely followed by the primary δ positions.

As already observed by Sarathy et al. [7] for iso-pentanol, the importance of the different reaction pathways is not sensitive to the equivalence ratio for both n-pentanol and iso-pentanol.

Following the observations of Figure 24 and Figure 25, predicted species profiles for the oxidation of stoichiometric fuel/O_2/Ar mixture at 1 atm and 1350 K analyzed at shock tube conditions are reported in Figure 27. Also in this case, n-pentanol oxidation directly proceeds through the formation of ethylene. On the contrary larger amounts of less reactive propylene are formed in iso-pentanol oxidation. Ethylene peaks later and is consumed correspondingly to ignition (represented by OH profile).

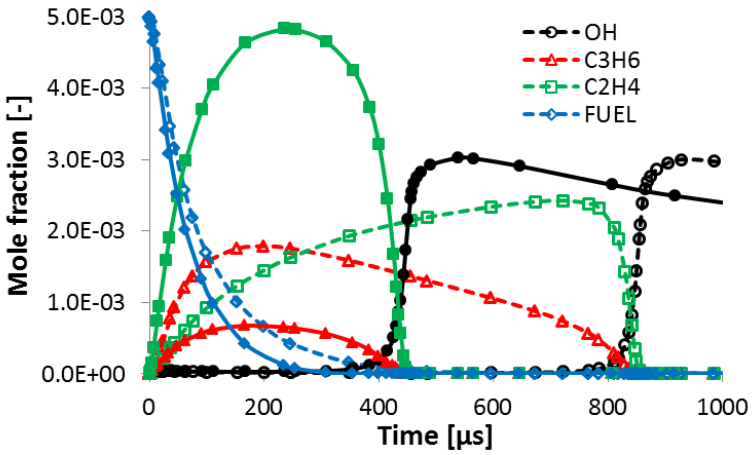

Figure 27: Predicted mole fractions of fuel and intermediate species as a function of time for the oxidation of a stoichiometric fuel/O_2/Ar mixture at 1 atm and 1350 K. Open symbols/dashed lines: iso-pentanol, Full symbols/solid lines: n-pentanol.

These considerations are also supported by the flux analyses of Figure 10 and 11. In fact, both the dominating H-abstraction channels in iso-pentanol oxidation (α and γ) lead to the formation of propylene, either directly (δ-radical decomposition) or through the formation of iso-propyl radical (α-radical decomposition). Moreover, as reported in Figure 28a sensitivity analyses carried out at the

same conditions of Figure 10 and 11, highlight how propylene specific reactions increase of importance moving from n-pentanol to iso-pentanol. Conversely n-pentanol is more sensitive to reactions involving ethylene, and mainly to the H-abstraction by OH reaction leading to the formation of reactive vinyl radical.

Finally, Figure 28b shows the most sensitive fuel specific reactions. The importance of H-abstractions by H and OH on δ and α sites is highlighted for both fuels. H-abstraction reactions contribute to a decreased reactivity (longer ignition delay times) by subtracting reactive radicals to the system. It is of interest to notice the opposite effect of dehydration reactions enhancing reactivity in the case of iso-pentanol and inhibiting reactivity for n-pentanol, and the positive contributions of unimolecular initiation reactions.

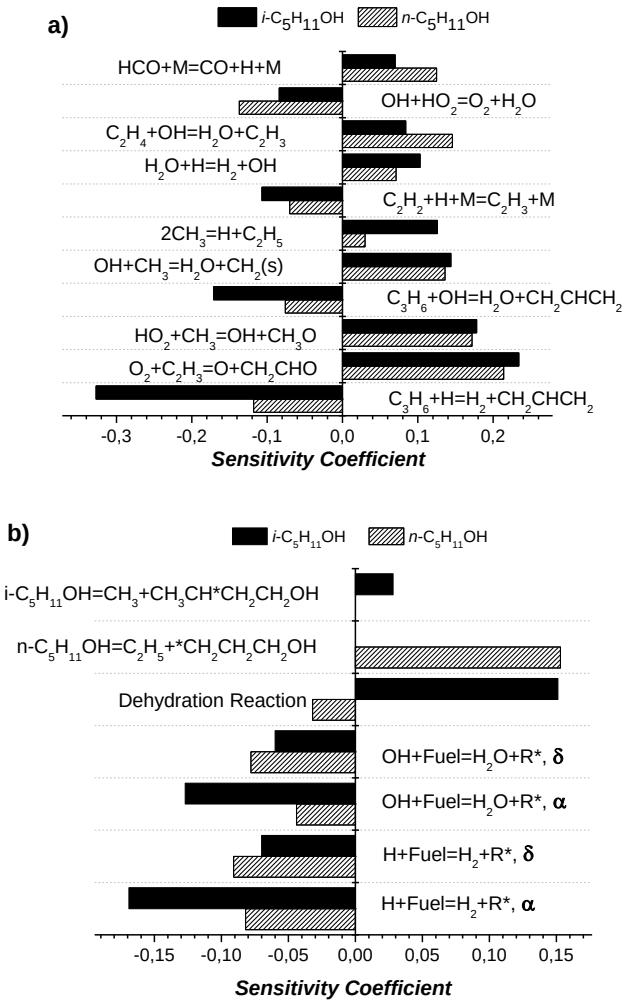

Figure 28: Sensitivity coefficients of ignition delay times to reaction rate coefficients, for 0.5% fuel/O_2/Ar stoichiometric mixtures at T=1350 K, p=1 atm. a) Most sensitive reactions belonging to the C_0-C_4 submechanism, b) most sensitive fuel specific reactions. A positive sensitivity coefficient stands for a reaction enhancing reactivity (shorter ignition delay time) and viceversa.

6 Conclusions

In the present work, laminar burning velocities of two pentanol isomers (*n*- and *iso*-pentanol) were rigorously obtained using the spherical bomb method. Three initial temperature were investigated for each fuel (353, 433 and 473 K) for equivalence ratio mixtures ranging from 0.7 to 1.5, at initial pressure of 1 bar. These new experimental results were compared with previous data from the literature. An overall good agreement was found for iso-pentanol flame speeds compared to the measurements of Sarathy et al. [7] but larger discrepancies were observed for n-pentanol flame speeds compared with those from Li et al. [3] and Togbé et al. [4]. These discrepancies were extensively analyzed and discussed. It was shown that laminar flame speeds for kinetic modeling evaluation are useful only if the initial conditions are well documented, especially the initial temperature corresponding to each run and more importantly the air composition. Only then a fair comparison between model and experiments can be made. A kinetic mechanism that describes the high temperature oxidation was developed and validated for both n- and iso-pentanol against laminar flame speeds from the present study. The mechanism consists of 230 species and 7885 reactions. The model was also tested with flame speeds from the literature. Larger deviations were observed for both *n*- and *iso*-pentanol for equivalence ratios > 1.0 when considering these data [3,4,7]. For a more complete validation, the mechanism was also tested with high temperature shock tube ignition data from Tang et al. [36]. Sensitivity analyses were performed highlighting important kinetic features. On the whole, a lower reactivity of iso-pentanol was observed both in the experimental measurements and in model predictions.

Acknowledgements

The authors are grateful for the financial support of this work provided by the French Ministry of Education and the French Labex CAPRYSSES (Cinétique chimique et aérothermodynamique pour des propulsions et des systèmes énergétiques propres et sûrs).

References

[1] Directive 2009/28/EC of the European Parliament and of the Council, http://eur-lex.europa.eu/LexUriServ/LexUriServ.do?uri=Oj:L:2009:140:0016:0062:en:PDF.

[2] S. M. Sarathy, P. Oßwald, N. Hansen, K. Kohse-Höinghaus, An experimental and kinetic modeling study of n-butanol combustion, Progress in energy and combustion science 44 (2014) 40-102.

[3] Q. Li, E. Hu, X. Zhang, Y. Cheng, Z. Huang, Laminar Flame Speeds and Flame Instabilities of Pentanol Isomer−Air Mixtures at Elevated Temperatures and Pressures, Energy and fuels 27 (2013) 1141-1150.

[4] C. Togbé, F. Halter, F. Foucher, C. Mounaim-Rousselle, P. Dagaut, Experimental and detailed kinetic modeling study of 1-pentanol oxidation in a JSR and combustion in a bomb, Proc. Combust. Inst. 33 (2011) 367-374.

[5] K. A. Heufer, S. M. Sarathy, H. J. Curran, A. C. Davis, C. K. Westbrook, W. J. Pitz, Detailed Kinetic Modeling Study of n‑Pentanol Oxidation, Energy and fuel 26 (2012) 6678-6685.

[6] G. Dayma, C. Togbe, P. Dagaut, Experimental and Detailed Kinetic Modeling Study of Isoamyl Alcohol (Isopentanol) Oxidation in a Jet-Stirred Reactor at Elevated Pressure, Energy and fuels 25 (2011) 4986-4998.

[7] S. M. Sarathy, S. Park, B. W. Weber, W. Wang, P. S. Veloo, A.C. Davis, C. Togbe, C. K. Westbrook, O. Park, G. Dayma, Z. Luo, M. A. Oehlschlaeger, F. N. Egolfopoulos, T. Lu, W. J. Pitz, C.-J. Sung, P. Dagaut, A comprehensive experimental and modeling study of iso-pentanol combustion, Combust. Flame 160 (2013) 2712-2728.

[8] A. Frassoldati, A. Cuoci, T. Faravelli, E. Ranzi, Kinetic modeling of the oxidation of ethanol and gasoline surrogate mixtures, Combustion Science and Technology 182 (2010) 653-667.

[9] A. Frassoldati, A. Cuoci, T. Faravelli, U. Niemann, E. Ranzi, R. Seiser, K. Seshadri, An experimental and kinetic modeling study of n-propanol and iso-propanol combustion, Combust. Flame 157 (2010) 2-16.

[10] R. Grana, A. Frassoldati, T. Faravelli, U. Niemann, E. Ranzi, R. Seiser, R. Cattolica, K. Seshadri, An experimental and kinetic modeling study of combustion of isomers of butanol, Combust. Flame 157 (2010) 2137-2154.

[11] A. Frassoldati, R. Grana, T. Faravelli, E. Ranzi, P. Oßwald, K. Kohse-Höinghaus, Detailed kinetic modeling of the combustion of the four butanol isomers in premixed low-pressure flames, Combust. Flame 159 (2012) 2295-2311.

[12] K. M. Van Geem, A. Cuoci, A. Frassoldati, S. P. Pyl, G. B. Marin, E. Ranzi, An experimental and kinetic modeling study of pyrolysis and combustion of acetone-butanol-ethanol (ABE) mixtures, Combustion Science and Technology 184 (2012) 942-955.

[13] M. Aghsaee, D. Nativel, M. Bozkurt, M. Fikri, N. Chaumeix, C. Schulz, Experimental study of the kinetics of ethanol pyrolysis and oxidation behind reflected shock waves and in laminar flames, Proc. Combust. Inst. 33 (2015) 393-400.

[14] Matlab, The MathWorks, Inc. Version 2012b. www.mathworks.com.

[15] F. Halter, T. Tahtouh, C. Mounaïm-Rousselle, Nonlinear effects of stretch on the flame front propagation, Combustion and flame 157 (2010) 1825-1832.
[16] P. Clavin, Dynamic behaviour of premixed flame fronts in laminar and turbulent flows, Progress in Energy and Combustion Science 11 (1985) 1-59.
[17] M. Matalon, B. J. Matkowsky, Flames as gasdynamic discontinuities, Journal of Fluid Mechanics 124 (1982) 239-259.
[18] P. D. Ronney, G. I. Sivashinsky, A Theoretical Study of Propagation and Extinction of Nonsteady Spherical Flame Fronts, J. of App. Math. 49 (1989) 1029-1046.
[19] R. C. Eschenbach, J. T. Agnew, Use of the constant volume bomb technique for measuring burning velocity, Combust. Flame 2 (1958) 273-285.
[20] COSILAB, The Combustion Simulation Laboratory, Version 3.3.2. http://www.SoftPredict.com. Rotexo GmbH & Co. KG, Haan, Germany, (2009).
[21] E. Varea, V. Modica, B. Renou, A.M. Boukhalfa, Pressure effects on laminar burning velocities and Markstein lengths for isooctane–ethanol–air mixtures, Proc. Combust. Inst. 34 (2013) 735-744.
[22] M.P. Burke, Z. Chen, Y. Ju, F. Dryer, Effect of cylindrical confinement on the determination of laminar flame speeds using outwardly propagating flames, Combust. Flame 156 (2009) 771-779.
[23] R. Mével, F. Lafosse, N. Chaumeix, G. Dupré, C.-E. Paillard, Spherical expanding flames in H2-N2O-Ar mixtures-Flame speed measurements and kinetic modeling, International Journal of Hydrogen Energy 34 (2009) 9007-9018.
[24] M. Pelucchi, K. P. Somers, K. Yasunaga, U. Burke, A. Frassoldati, E. Ranzi, H. J. Curran, T. Faravelli, Experimental and kinetic modeling study of C3-C5 n-aldehydes auto-ignition and pyrolysis in shock tube, Combust. Flame 162 (2015) 265-286.
[25] L. Zhao, L. Ye, F. Zhang, L. Zhang, Thermal Decomposition of 1-Pentanol and Its Isomers: A Theoretical Study, The Journal of Physical Chemistry A 116 (2012) 9238-9244.
[26] S. M. Sarathy, P. Oßwald, N. Hansen, K. Kohse-Höinghaus, Alcohol combustion chemistry, Progress in Energy and Combustion Science 44 (2014) 40-102.
[27] E. Ranzi, M. Dente, T. Faravelli, G. Pennati, Prediction of Kinetic Parameters for Hydrogen Abstraction Reactions, Combustion Science and Technology 95 (1993) 1-50.
[28] H. J. Curran, Rate constant estimation for C1 to C4 alkyl and alkoxyl radical decomposition, International Journal of Chemical Kinetics 38 (2006) 250-275.
[29] E. Ranzi, M. Dente, A. Goldaniga, G. Bozzano, T. Faravelli, Lumping procedures in detailed kinetic modeling of gasification, pyrolysis, partial oxidation and combustion of hydrocarbon mixtures, Progress in Energy and Combustion Science 27 (2001) 99-139.
[30] M. Dente, G. Bozzano, T. Faravelli, A. Marongiu, S. Pierucci, E. Ranzi, In Advances in Chemical Engineering, B. M. Guy Ed., Academic Press, 2007, p 51-166.
[31] J. Moc, J. M. Simmie, H. J. Curran, The elimination of water from a comformationally complex alcohol: A computational study of the gas phase dehydration of n-butanol, Journal of Molecular Structure 928 (2009) 149-157.
[32] A. Cuoci, A. Frassoldati, T. Faravelli, E. Ranzi, Computer Physics Communications 2015. DOI: 10.1016/j.combustflame.2009.06.023

[33] A. Cuoci, A. Frassoldati, T. Faravelli, E. Ranzi, Formation of soot and nitrogen oxides in unsteady counterflow diffusion flames, Combust. Flame 156 (2009) 2010-2022

[34] E. Ranzi, A. Frassoldati, R. Grana, A. Cuoci, T. Faravelli, A. Kelley, C. Law, Hierarchical and comparative kinetic modeling of laminar flame speeds of hydrocarbon and oxygenated fuel, Progress in Energy and Combustion Science 38 (2012) 468-501.

[35] M. Smooke, H. Rabitz, Y. Reuven, F. Dryer, Application of Sensitivity Analysis to Premixed Hydrogen-Air Flames, Combustion Science and Technology 59 (1988) 295-319.

[36] C. Tang, L. Wei, X. Man, J. Zhang, Z. Huang, C. K. Law, High temperature ignition delay times of C5 primary alcohols, Combust. Flame 160 (2013) 520-529.